Results in Engineering 27 (2025) 106222

Contents lists available at ScienceDirect

Results in Engineering

journal homepage: www.sciencedirect.com/journal/results-in-engineering

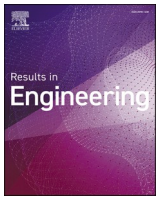

Research paper

Sustainable clay-based materials stabilised by low-temperature treatments: Salt degradation and chemomechanical approach

Marta Cappai [a,b], Giorgio Pia [a,b,*]

[a] Dipartimento di Ingegneria Meccanica, Chimica e dei Materiali, Università degli Studi di Cagliari, Piazza d'Armi, Cagliari 09123, Italy
[b] Materialia Association, San Gavino Monreale, Sardinia 09037, Italy

ARTICLE INFO

Keywords:
Clay-based materials
Stabilization
Thermal treatment
Salt resistance
Chemomechanical model

ABSTRACT

Earthen materials represent a low environmental impact alternative, but they are inherently vulnerable to water exposure and degradation processes. For this reason, they often require stabilization through thermal treatments. In this study, temperatures lower than those typically used for ceramic firing were applied, with the aim of preserving the sustainability of the final products. However, while the treated structures exhibit improved water resistance, new degradation mechanisms typical of construction materials, such as salt crystallization, may arise. To investigate this aspect, an experimental campaign has been carried out to assess the resistance to sodium sulfate salt crystallisation. The results have been compared with predictions from a chemomechanical model, which has been adapted in this work through the introduction of a porosity activation factor. The model has been shown to be effective in predicting the onset cycle of degradation, offering a valuable tool for the design of more durable and resilient materials.

1. Introduction

The construction sector is one of the main contributors to greenhouse gas emissions and global energy consumption, significantly impacting climate change and the depletion of natural resources. According to the 2023 report by International Energy Agency, the construction sector is responsible for nearly 37% of global carbon dioxide (CO_2) emissions, with 11% attributed to building materials such as cement, steel, and aluminum [1]. While energy efficiency strategies have helped reduce operational emissions from buildings, the embodied emissions in construction materials remain a critical challenge for the sector [2]. To achieve the sustainability goals set by the European Union and key international decarbonization strategies, it is essential to develop low-impact solutions [3,4].

Conventional materials such as cement and steel have a high environmental impact. Portland cement, in particular, accounts for about 7% of global CO_2 emissions, with a significant portion resulting from the calcination of limestone and the high-temperature processing required for its production. Similarly, the production of steel and aluminum involves highly energy-intensive and polluting processes [2,5,6]. Mitigation strategies implemented so far have focused on energy efficiency and carbon capture, yet significant challenges remain in reducing emissions from material production [7–10]. In this context, the search for alternative construction materials becomes essential for a more sustainable built environment, emphasizing the integration of low-impact materials into contemporary construction practices without compromising mechanical performance and structural durability [2,8].

Among these, clay-based materials are emerging as a promising solution due to their low embodied energy, local availability, and high recyclability [11–20]. However, their large-scale adoption is hindered by technical challenges that limit their widespread use and regulatory acceptance [21–25]. Clay-based construction materials, such as adobe, rammed earth, and compressed earth blocks, represent a sustainable construction alternative with significant potential. These materials exhibit lower embodied energy compared to industrial materials, excellent hygrothermal regulation properties, and high recyclability. Furthermore, their local availability facilitates on-site production, thereby reducing transportation costs and associated emissions [23, 26–32]. However, a major limitation of clay-based materials is their sensitivity to water and susceptibility to degradation, which can significantly impact the long-term durability of structures [33–37].

To enhance the strength of clay-based materials, various stabilization techniques have been developed. Among these, the addition of cement increases mechanical strength but compromises sustainability and

* Corresponding author at: Dipartimento di Ingegneria Meccanica, Chimica e dei Materiali, Università degli Studi di Cagliari, Piazza d'Armi, Cagliari 09123, Italy.
E-mail address: giorgio.pia@dimcm.unica.it (G. Pia).

https://doi.org/10.1016/j.rineng.2025.106222
Received 3 June 2025; Received in revised form 1 July 2025; Accepted 8 July 2025
Available online 9 July 2025

material reversibility, as it introduces components that are difficult to remove and recycle [38–42]. Real et al. [41] investigated the use of thermoactivated recycled cement as an eco-efficient stabiliser for compressed earth blocks, partially replacing ordinary Portland cement. The study demonstrated that thermoactivated recycled cement significantly enhanced mechanical strength and refined the microstructure, with hygroscopic behavior comparable to ordinary Portland cement stabilised compressed earth blocks. However, due to its high water demand, thermoactivated recycled cement reduced block compactness and strength relative to ordinary Portland cement, and its effectiveness remains sensitive to soil type and porosity [41]. The use of specific amounts of lime reduces water sensitivity and improves durability; however, its production remains highly energy-demanding, with remarkable environmental consequences [43–46]. Malkanthi et al. [45] evaluated lime and lime–cement combinations for stabilizing compressed earth blocks made from soils with low clay and silt content. While lime alone improved workability and mechanical properties, only the addition of cement allowed the blocks to meet structural standards. However, the use of cement, an energy-intensive material, partially offsets the environmental benefits of earth construction. Moreover, the study is limited to short-term results and a narrow range of soil types [45].

The incorporation of synthetic polymers enhances moisture resistance and structural integrity, but it limits recyclability, may lead to the release of pollutants into the environment, and is derived from fossil-based sources [47–49]. Park et al. [49] investigated the stabilizing effect of acrylic polymer and epoxy emulsion on red clay and sand, including their mixtures, with and without lime addition. The study identified optimal binder compositions that significantly improved unconfined compressive strength—especially when lime was used—through enhanced bonding and microstructural densification. However, the performance was highly sensitive to material ratios and moisture content, and the use of synthetic polymers raises environmental concerns regarding long-term sustainability [49]. The stabilization of earth materials using biopolymers and other bio-based polymers has been the subject of extensive research, aiming to improve both mechanical performance and water resistance while maintaining environmental compatibility [46,47,50–64]. Despite promising improvements in mechanical strength and water resistance, the use of biopolymers in earth stabilization presents several limitations, including high sensitivity to soil composition, lack of standardized testing protocols, and limited understanding of long-term durability and biodegradability under varying environmental conditions [51].

Other promising techniques are based on biomineralization and nanomodification of clay-based materials [52,65–73]. Bernat-Maso et al. [66] investigate the influence of microbially induced calcium carbonate precipitation (MICP) using *Sporosarcina pasteurii* on the mechanical performance of compressed earth blocks. Results indicate that bacterial activity can enhance apparent cohesion in sandy soils cured in high humidity. However, in well-graded soils, bacterial activity reduced strength due to decreased particle interlocking and void formation associated with bacterial sporulation, emphasizing the role of pore structure and curing environment [66]. Akturk et al. [72] investigated the bio-stabilization of rammed earth using three calcite-precipitating microorganisms (*Bacillus subtilis, Sporosarcina pasteurii*, and *Bacillus subtilis* subsp. *subtilis*), combined with lime and gypsum. Their results showed that, in stabilized mixes, bacterial incorporation at optimal concentrations significantly increased compressive strength due to calcite formation. However, no strength gain was observed in unstabilized soils, highlighting the necessity of calcium sources and suitable growth conditions for microbial activity [72]. Karozou et al. [73] explored the use of nano-additives, specifically nanoclay, nanosilica, and nanoalumina, to improve the physical and mechanical properties of clay mortars. Their findings showed that nanoclay notably enhanced compressive and flexural strength and cohesion, while the nanosilica and nanoalumina combination was less effective, resulting in structural weaknesses and high shrinkage. However, the study was limited to small-scale laboratory tests and did not assess long-term durability or environmental interactions under real conditions [73]. Niroumand et al. [69] reviewed the potential of nanotechnology to enhance the performance of rammed earth walls, highlighting the role of nano-clays. Their case study demonstrated that nano-clay incorporation can increase compressive strength by up to 2.2 times compared to conventional mixes, also improving heat resistance and cohesion. However, the findings are based on preliminary investigations and lack standardized testing and long-term durability assessment under real-world conditions [69].

While these high-performance techniques can enhance specific material properties, they often require the use of synthesized additives, complex protocols, or longer processing times, factors that typically result in higher energy demand and limited applicability in real-world construction scenarios, especially in low-resource or heritage conservation contexts.

These limitations highlight the need for alternative solutions capable of increasing strength without compromising sustainability, promoting the adoption of less impactful stabilization processes that are more compatible with bio-based construction. A valid alternative for the stabilization of earthen materials is represented by thermal treatments, especially when applied at low temperatures. This method offers several advantages, including reduced energy consumption compared to traditional firing techniques, the preservation of environmental sustainability by avoiding the use of cement and synthetic polymers, and the improvement of mechanical properties through increased internal cohesion [74,75].

Previous studies have demonstrated that thermal treatments not only enhance mechanical strength but also improve water resistance and surface strength, making them a viable alternative to chemical stabilization methods [74–76].

Stabilization through low-temperature thermal treatments initiates early ceramization processes that, while enhancing mechanical strength and water resistance, also introduce degradation mechanisms characteristic of traditional ceramic materials. Among these, one of the most significant is salt crystallisation [77–85] which is considered a major factor in the deterioration of porous materials used in historical and contemporary construction [79,82,86–96]. The phenomenon occurs due to the infiltration and evaporation of aqueous solutions containing dissolved salts, which then precipitate and accumulate in the porous structure of the materials.

The effect of cyclic salt crystallization varies depending on the salt type. Among the different types of salts that can cause deterioration in building materials, sodium sulfate is widely recognized for its destructive potential due to its high crystallization pressure and phase transitions. It can crystallize in different forms, with the most common in construction materials being thenardite (anhydrous phase, expressed as Na_2SO_4) and mirabilite (hydrated phase, expressed as $Na_2SO_4{\cdot}10H_2O$) [97–102]. The cyclic phase transitions between hydrated and anhydrous salt forms generate expansive pressures that can cause cracking, scaling, and even complete disintegration of the material [87–89,100,103–107]. Indeed, the hydration process of mirabilite leads to a substantial volumetric expansion of 314% [102], generating mechanical stresses that can severely compromise the material's stability by causing internal cracking and loss of structural integrity, similar to the deterioration observed in natural stone and other porous materials [97–102]. The crystallisation pressure exerted by sodium sulfate has been quantified in various studies, indicating that it can exceed the tensile strength of many construction materials, leading to irreversible damage [102,108,109]. In particular, the transition from thenardite to mirabilite is highly sensitive to environmental conditions, especially relative humidity, which means that even slight variations in climate can significantly accelerate degradation processes [100,109]. This makes the study of salt crystallisation effects crucial not only for historical conservation but also for modern sustainable construction materials.

To assess the resistance of low-temperature stabilized materials to salt crystallisation, a degradation test was performed using sodium sulfate (Na_2SO_4) crystallisation cycles. The experimental procedure involved cyclic immersion in a sodium sulfate solution followed by controlled drying phases, inducing repeated crystallisation and dissolution processes within the porous matrix. These conditions enhance the effects of salt action, subjecting the material to significant internal stresses that can lead to microcracking, material loss, and progressive structural weakening. By monitoring weight variations throughout the cycles, it is possible to quantify the extent of degradation.

The materials analyzed in this study are composed of a clay-rich matrix combined with recycled aggregates from building demolitions allowing the reduction of virgin raw material. The stabilization of the materials was carried out through low-temperature thermal treatments, below the firing temperature of traditional ceramics, to enhance durability. This approach not only significantly reduces the energy demand compared to conventional stabilization processes (such as those based on cement or lime) but also contributes to a circular economy strategy by reintroducing construction waste into the material cycle [18]. These aspects align with current goals in sustainable construction and support the relevance of the proposed materials for real-world scenarios.

In order to assess the resistance to salt crystallisation, a degradation test was performed using sodium sulfate (Na_2SO_4) crystallisation cycles. The experimental procedure involved cyclic immersion in a sodium sulfate solution followed by controlled drying phases, inducing repeated crystallisation and dissolution processes within the porous matrix. These conditions enhance the effects of salt action, subjecting the material to significant internal stresses that can lead to microcracking, material loss, and progressive structural weakening. By monitoring weight variations throughout the cycles, it is possible to quantify the extent of degradation.

The obtained results will be compared with the predictions from the modified model proposed by Flatt et al. [81,109]. This model estimates the quantity of crystallisation cycles at which a material can reach a critical stress threshold that leads to damage. By integrating porosimetric data and mechanical properties, the model quantifies the internal stresses induced by sodium sulfate crystallisation and compares them with the material's tensile strength to determine the point of structural failure [109]. This model provides a predictive tool for assessing the durability of stabilized materials in environments exposed to sodium sulfate induced decay. The comparison between experimental data and theoretical predictions will help evaluate the model's reliability and its potential for guiding material selection in sustainable construction applications. This comparison aims to assess the model's predictive accuracy and extend its applicability to this class of materials, further validating its robustness in simulating degradation phenomena.

2. Materials and methods

Clay and recycled aggregates have been used for the mix design of experimental materials. The clay, sourced from a quarry in Lozzolo, Vercelli (Italy), is composed of quartz, albite, illite, interstratified illite/montmorillonite, interstratified illite/chlorite, and traces of kaolinite. Recycled aggregates have been provided by R.E.R. Srl (Is Seddas – Quartucciu – Sardinia – Italy) and they consist mainly of quartz, calcite, feldspar, muscovite/illite, and kaolinite. The recycled aggregates have undergone a cleaning process to remove contaminants such as plastic and wood. This process has involved repeated immersion in distilled water with agitation, followed by manual removal of floating impurities. The procedure has been repeated until no visible contaminants remained. After the cleaning process, the recycled aggregates have been dried in an oven at 100 °C for 24 h and then sieved to retain only particles smaller than 2 mm. Sodium sulfate (CAS 7757–82–6), used for salt crystallisation cycles, was purchased from Sigma-Aldrich (Merck, Darmstadt, Germany).

The systems have been formulated in varying weight proportions using distilled water:

- A: 4 parts clay, 4 parts recycled aggregates, 2 parts water;
- B: 3 parts clay, 5 parts recycled aggregates, 2 parts water;
- C: 2 parts clay, 6 parts recycled aggregates, 2 parts water.

Additional mix designs with different proportions have also been tested, revealing that clay contents greater than 4 parts led to excessive shrinkage of the samples, whereas contents lower than 2 parts resulted in lower cohesion.

The raw materials have been dried for 24 h at 105 °C in an oven, then mixed in dry state and homogenized for approximately 1 min. Water has been gradually added, and the compound has been mixed using an electric mixer for about 5 min. After mixing, the material has been allowed to rest for 5 min, mixed again for an additional 30 s, and subsequently placed into cylindrical metal molds (internal diameter of 45 mm, height of 6 mm) for the specimens used in water resistance and salt crystallisation cycle tests, and into prismatic molds (20 × 20 × 100 mm) for mechanical testing. The specimens have been initially air dried under laboratory conditions for 48 h, followed by a 30 day curing period in a desiccator. Dimensional shrinkage has been assessed by measuring changes in diameter and height using a caliper. After drying, samples A exhibited the highest average diameter reduction (2.92 ± 0.03%). Samples B and C showed average diameter reductions of 2.58 ± 0.12% and 1.67 ± 0.10%, respectively. Systems with higher recycled aggregates content exhibited lower shrinkage, as the aggregates act as the structural framework of the composite.

To evaluate the effects of thermal stabilization, the samples have been treated at 400 °C, 450 °C, 500 °C, 550 °C, and 600 °C for 10 min each by using a Carbolite STF 15/450 tubular furnace (Carbolite Gero GmbH & Co. KG, Germany). For each thermal treatment studied, 18 samples have been produced. Mineralogical composition has been analysed by X-ray diffraction (XRD) using a Bruker D8 Advance diffractometer (Leipzig, Germany) with a LYNXEYE XE-T multi-mode detector and Cu Kα radiation.

To evaluate water resistance, the samples have been pre-conditioned in an oven at 105 °C and subsequently immersed in distilled water for 360 min. Water absorption has been monitored over time by measuring weight variation, and the time until decohesion has been recorded as an indicator of water resistance. The test has been performed on 3 samples for each thermal treatment tested. In order to study porosity microstructure, mercury intrusion porosimetry (MIP) has been carried out (three times per sample) using a Micromeritics® Autopore IV 9500 lab instrument (conditions: 2200 bars; equilibration time: 10 s). In addition, the morphology of the samples has been investigated using a scanning electron microscope (SEM) ESEM FEI Quanta 200. An MTS Landmark 370 universal testing system (Eden Prairie, MN, USA) has been employed to conduct tensile stress measurements during the mechanical testing phase.

The resistance to salt crystallisation has been tested using a cyclic accelerated degradation procedure (n_c indicates the number of cycles) schematically represented in Fig. 1 [109]. The samples have been dried (105 °C for 24 h); subjected to cycles consisting of immersion in a 6.1% sodium sulfate solution for 1 h at 20 °C; dried in a muffle furnace at 105 °C for 18 h; weighed to evaluate the mass variation (Δm). According to Flatt et al., it has been assumed that the beginning of salt crystallisation-induced degradation occurs when at least 50% of the samples in the same system have exhibited a mass loss compared to their initial dry mass [109]. The experimental campaign was interrupted when all samples showed a weight loss relative to their initial dry mass.

The 6.1% sodium sulfate concentration and the entire procedure replicate the methodology applied by Flatt et al. [109]. A total of 12 samples have been tested for each treatment temperature.

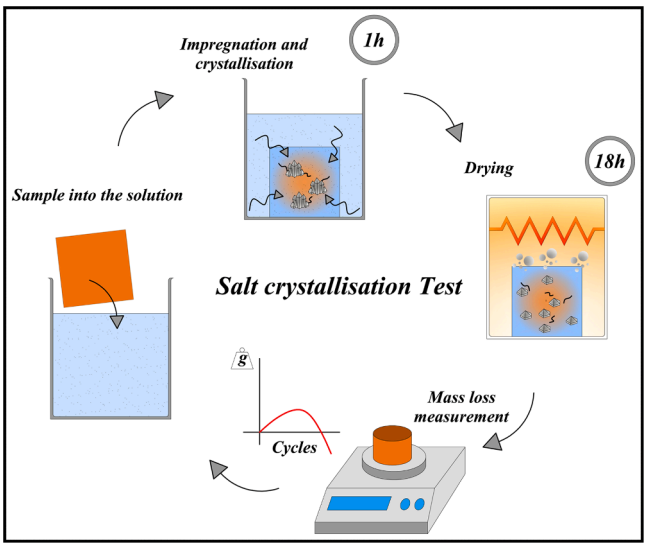

Fig. 1. Scheme of salt crystallisation test.

3. Results and discussion

Three different mix designs have been subjected to thermal treatment at 450, 500, 550, and 600 °C for 10 min. From a practical perspective, brief treatments are more compatible with real-world constraints, especially in on-site applications, where time and energy availability are often limited. Prolonging the thermal exposure significantly increases energy consumption, which could undermine the environmental advantage of low-temperature stabilization. XRD analysis shows the variation in mineralogical composition with increasing temperature (Fig. 2). Thermal treatment induced significant changes in the clay minerals, as evidenced by the progressive decrease in the intensity of basal reflections with increasing temperature. Starting from 500 °C, the peaks associated with kaolinite disappeared due to the collapse of its crystalline lattice [110,111]. At 600 °C, the intensity of low-angle peaks related to mixed-layer phases such as illite/montmorillonite and interstratified illite/chlorite had almost completely disappeared.

MIP tests show that, for different systems (A, B, C), porosity increases proportionally to the increase of recycled aggregates content (Table 1 and Fig. 3). Moreover, samples treated at diverse temperatures, porosity increases when temperature increases. By considering a determined temperature, for example 600 °C, average porosity is equal to 22.76, 25.35, 28.55% respectively for A, B, C. While, for example in system A, average percentage porosity has values of 20.11, 21.87, 22.08, 22.76% respectively for samples treated at 450, 500, 550 and 600 °C (Table 1).

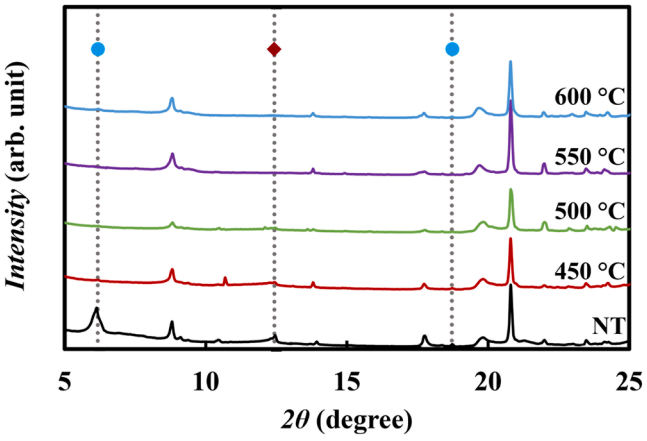

Fig. 2. XRD pattern of untreated (NT) and heat-treated sample A at different temperatures. The kaolinite peak (◆) is no longer visible starting from 500 °C, while the peaks associated with mixed phases such as illite/montmorillonite and interstratified illite/chlorite (●) progressively decrease in intensity with increasing temperature, disappearing completely at 550 °C.

A detailed analysis of porosimetric data makes it possible to determine the pore size distribution in relation to the characteristic dimensions of the pores. This information is particularly relevant in the context of salt crystallisation, for which it is possible to identify a porosity range defined as critical. Specifically, this refers to pore sizes where the crystallisation phenomenon is intense enough to cause damage to the material's microstructure. In the literature, various values of critical pore size are reported, below which salt crystallisation of sodium sulfate becomes significant [82]. These values have been obtained either experimentally or through analytical procedures and generally fall within the range of 0.05–5 μm [77,112–118]. For these reasons, in this study, the entire range of pore sizes below 5 μm was assumed to represent the critical porosity.

Experimental pore size distributions obtained in this work, such as those reported in Fig. 3 for system A, show a remarkable mercury absorption in correspondence of greater pores. By considering pore size critical range lower to 5 μm (reported in red in Fig. 3), consequent average critical porosity is equal to 6.5, 7.81 and 9.16% respectively for A, B and C. These values correspond to about 30.07, 32.28 and 34.00% of the total porosity of A, B and C.

In order to verify the pore size, and in particular the critical pore range, SEM inspections were performed. Fig. 4a–c shows micrographs representing the typical structure of samples from systems A, B, and C, respectively at 600 °C. It is possible to observe pores with sizes both larger and smaller than the critical radius.

Tensile strength values are also reported in Table 1. As expected, the variation is related to porosity. For the specific thermal treatment, as porosity increases, tensile strength decreases. Values vary in a small range between 0.460 and 1 MPa, 0.423 and 0.985 MPa, and 0.415 and 0.858 MPa respectively for systems A, B, and C across the corresponding treatment temperatures.

Considering specific mix designs under different thermal treatments, it is possible to observe that as porosity increases, tensile strength also increases. For example, considering series A: at 450 °C, porosity is 20.11 ± 0.76 and tensile strength is 0.460 ± 0.061 MPa; at 500 °C, porosity is 21.87 ± 1.22 and tensile strength is 0.599 ± 0.120 MPa; at 550 °C, porosity is 22.08 ± 0.98 and tensile strength is 0.901 ± 0.080 MPa; finally, at 600 °C, porosity is 22.76 ± 0.98 and tensile strength is 1.003 ± 0.502 MPa. This behavior is related to the fact that at temperatures approaching 450 °C, kaolinite begins to undergo dehydroxylation, resulting in the partial collapse of its layered structure and initiating the transformation toward metakaolinite. Although this transformation is in the initial stage, it already alters the clay matrix, affecting both the morphology and connectivity of the pore network. Illite, though more thermally stable, also experiences early structural disorder and partial dehydroxylation around 500–600 °C, which leads to a weakening of its crystalline framework and the formation of more reactive, disordered phases. These changes, albeit incipient, contribute to an enhancement of the internal bonding between particles and phases, thus improving the overall tensile response of the material. Similar effects have been observed in thermally treated clay materials, where increased porosity due to mineral transformations coexists with improved strength. For instance, Nigay et al. [119] and Atzeni et al. [76] demonstrated that dehydration and dehydroxylation in the range of 400–600 °C can lead to morphological restructuring and surface activation that increase porosity while simultaneously enhancing mechanical performance.

In every case, standard deviation is relatively high, which can be attributed to several interacting factors related to the nature of the materials and the experimental procedure. First, the intrinsic heterogeneity of the composite plays a key role. Clays and recycled aggregates used in the mix present a natural variability in terms of shape, density,

Table 1
Tensile strength, global pore volume percentage, critical pore percentage, for systems treated at different temperatures and with diverse mix-designs.

T (°C)	A			B			C			R (ε_{tot} - σ_T)
	ε_{tot} (%)	$\varepsilon_{r>5\ \mu m}$ (%)	σ_T (MPa)	ε_{tot} (%)	$\varepsilon_{r>5\ \mu m}$ (%)	σ_T (MPa)	ε_{tot} (%)	$\varepsilon_{r>5\ \mu m}$ (%)	σ_T (MPa)	
450	20.11 ± 0.76	5.97 ± 0.60	0.460 ± 0.061	22.59 ± 0.75	6.98 ± 0.71	0.423 ± 0.063	26.70 ± 0.75	8.73 ± 0.91	0.415 ± 0.055	- 0.8785
500	21.87 ± 1.22	6.54 ± 0.37	0.599 ± 0.120	24.52 ± 1.16	7.98 ± 1.04	0.585 ± 0.055	27.27 ± 1.16	9.06 ± 0.64	0.525 ± 0.075	- 0.9448
550	22.08 ± 0.98	6.58 ± 0.59	0.901 ± 0.080	24.85 ± 0.63	8.07 ± 0.74	0.870 ± 0.090	27.61 ± 0.63	9.68 ± 0.93	0.802 ± 0.080	- 0.9773
600	22.76 ± 2.03	7.03 ± 0.92	1.003 ± 0.502	25.35 ± 0.46	8.39 ± 0.98	0.985 ± 0.045	28.55 ± 0.46	9.99 ± 1.03	0.859 ± 0.048	- 0.9401
R (ε_{tot} - σ_T)	0.8851			0.8994			0.9091			

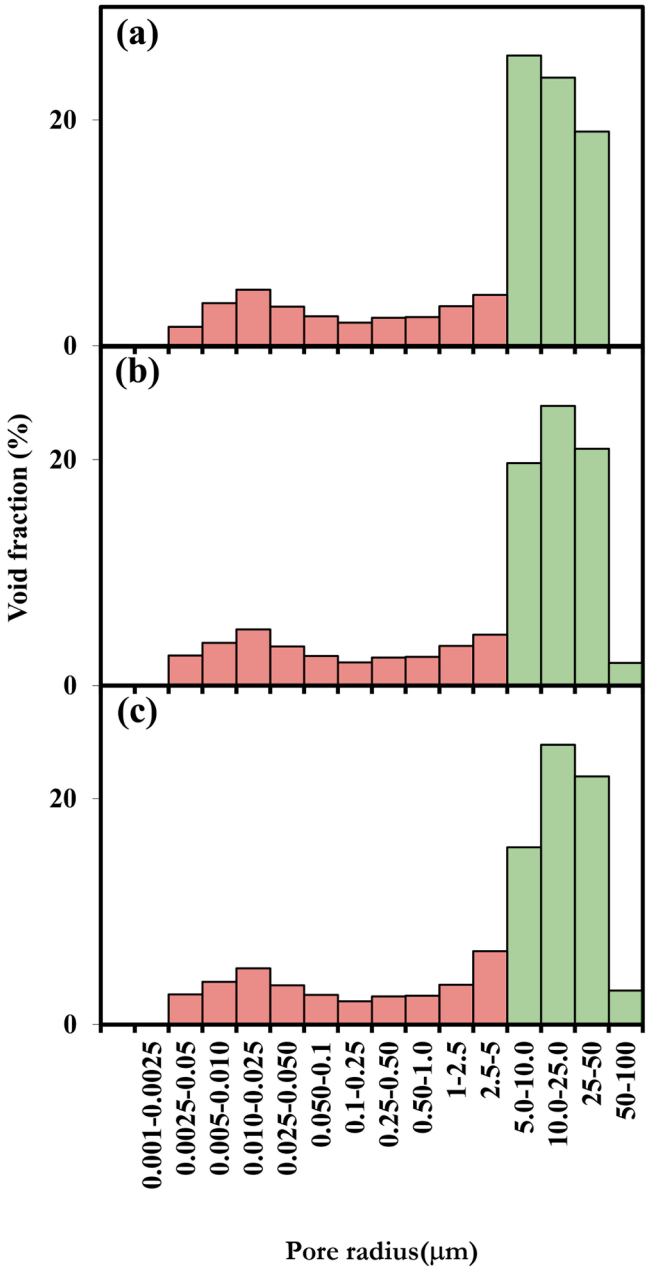

Fig. 3. Pore size distribution for system A (a), B (b) and C (c) at 450 °C. The volumetric fraction of pores within the critical radius is shown in red. The remaining pore fraction is shown in green.

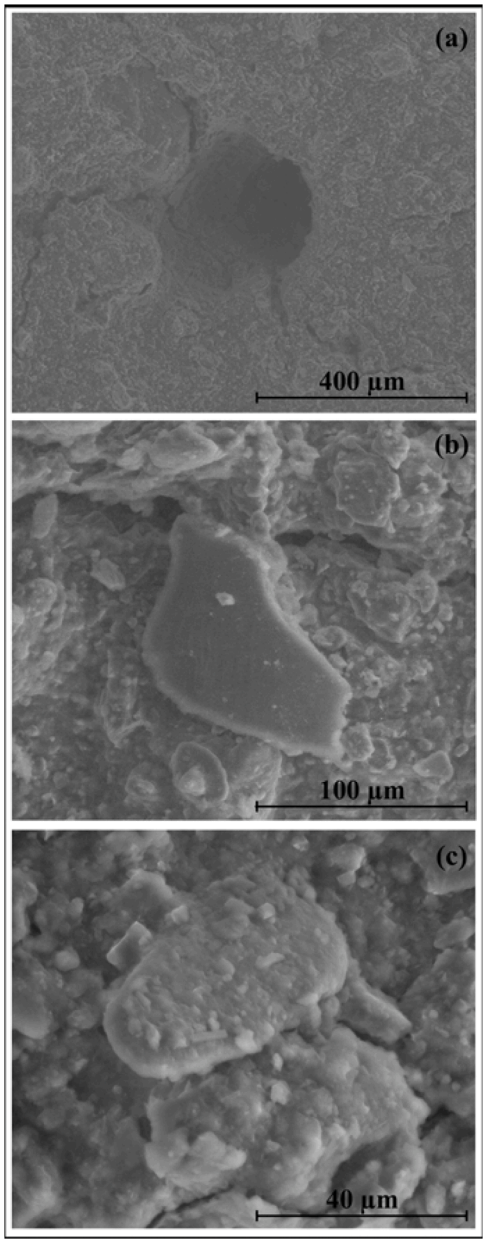

Fig. 4. SEM images of samples from A (a), B (b) and C (c) systems at 600 °C.

and surface morphology, which influences the formation of the internal microstructure and the distribution of stress during mechanical testing. Even with careful control of the mix proportions, small fluctuations can also affect workability and compaction, leading to localized differences

in material cohesion. Second, although the sample preparation protocol was standardized, the manual component of the process inevitably introduces variability. Slight inconsistencies in compaction force or mixing uniformity, due to human handling, can result in subtle but significant differences across samples, especially in systems with low internal cohesion. Moreover, it is important to consider that the tensile strength values under investigation are inherently low. At this scale, even small microstructural differences can result in relatively large deviations when expressed as standard deviation values. This heterogeneity is also reflected in the literature [120–124].

To assess the effectiveness of thermal treatments as stabilizers for the different systems, total immersion tests have been performed by submerging the samples in distilled water for up to 360 min. Only samples A450, B450, C450, and C500 showed mass loss after 140, 120, 8, and 260 min, respectively. All other samples completed the 360-minute test without detachment, cracking, or any resulting weight loss. The higher recycled aggregates content in the studied mix designs confirms the structural weakening observed through mechanical testing and the increase in porosity.

The thermal treatments therefore stabilized the structure; however, although their sensitivity to water and water-related forms of degradation has decreased, the resulting microstructures may now be susceptible to other typical degradation mechanisms of porous building materials, such as those caused by sodium sulfate crystallisation.

During the salt crystallisation test, samples initially gain weight due to the accumulation of salt within the porous matrix (Fig. 5). The cyclic transformation between the sodium sulfate phases thenardite and mirabilite leads to volume changes inside the pores, which over time cause damage such as detachment and material loss. These effects become experimentally evident through the measured decrease in the sample's weight. In Fig. 5, the X-coordinate of the filled symbols represents the cycle at which 50% of the specimens exhibited measurable mass loss compared to their initial dry weight (according to Flatt et al. [109]).

The resistance of the material to salt crystallisation is strongly influenced by thermal treatment temperature, mechanical properties, and porosity, all of which are closely linked to the mix design. At the same thermal treatment temperature, macroscopic behavior can be attributed to microstructural differences induced by varying recycled aggregate contents. As the amount of recycled aggregate increases, the material progressively loses cohesion and exhibits diminished mechanical strength, resulting in greater susceptibility to degradation. This trend is clearly reflected in Fig. 5, where systems with higher recycled aggregate content display increased sensitivity to expansive phenomena. Specifically, sodium sulfate crystallisation induces internal stresses that exceed the local mechanical limits of the matrix, leading to surface detachment and consequent mass loss. The number of salt crystallisation cycles required to induce significant mass loss decreases with increasing porosity and decreasing tensile strength. By comparing the data from Table 1 and Fig. 3, a progressively higher susceptibility to salt crystallisation-induced damage is evident in systems A, B, and C. System A consistently demonstrates the highest resistance, with at least 50% of samples showing mass loss (compared with their initial dry weight) after 4 cycles at 450 °C, 5 at 500 °C, and 7 at both 550 °C and 600 °C. System B follows a similar trend, while system C, characterized by higher critical porosity and lower tensile strength, shows earlier onset of degradation under the same conditions.

The possibility of studying this phenomenon not only experimentally but also through an analytical procedure is of particular interest. The high variability of the properties of the earth-based materials investigated - depending on the mix design and thermal treatment temperatures - can be effectively addressed through modelling, which may support the standardization of processes and the prediction of the material's service life. Particularly relevant in this context is the model developed by Flatt et al. [109], which has been formalized to predict salt degradation resistance, in terms of the number of cycles a material can withstand due to phase transitions of sodium sulfate. Specifically, this

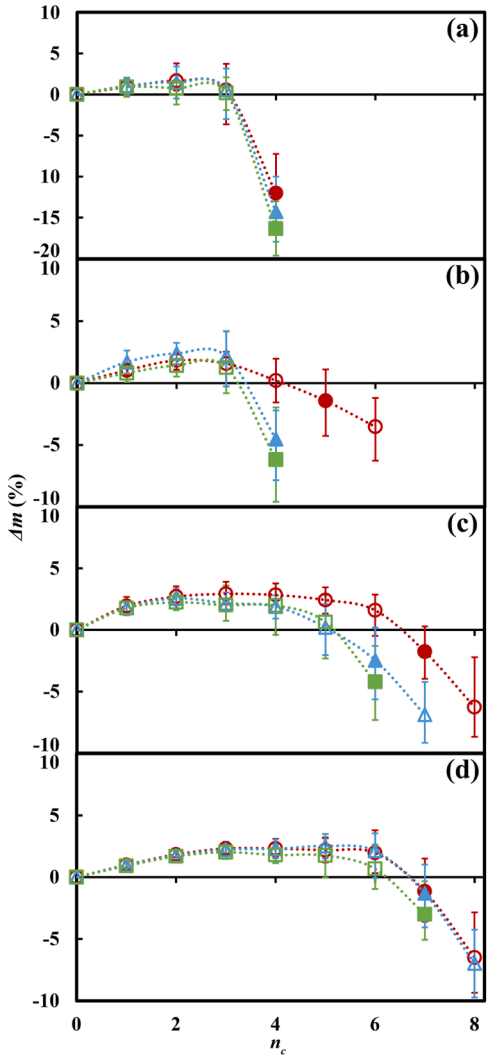

Fig. 5. Mass variation of samples A (°), B (△), and C (□) at temperatures: (a) 450 °C; (b) 500 °C; (c) 550 °C; (d) 600 °C. The x-axis indicates the number of cycles (n_c). Filled points indicate cycles at which at least 50% of the samples have lost mass compared to their initial dry weight [109].

approach is based on the progressive saturation of the pore network with sodium sulfate, leading to the development of crystallisation pressure (ΔPc), defined by:

$$\Delta P_C = \frac{RT}{\bar{\nu}_M}\left[K_{sp,T} - K_{sp,M} + 10ln\left(\frac{RH_{sat,T}}{100}\right)\right] \quad (1)$$

Here, R (8.314 J • mol^{-1} • K^{-1}) is the ideal gas constant, T (293.15 K) is the reference temperature, and $\bar{\nu}_M$ represents the molar volume of mirabilite, equal to 217.7 cm^3•mol^{-1}. The terms $K_{sp,T}$ and $K_{sp,M}$ refer to the thermodynamic solubility products of thenardite and mirabilite, respectively [97]. The relative humidity at which thenardite begins to deliquesce, absorbing moisture from the surrounding atmosphere and dissolving into an aqueous phase, is indicated as $RH_{sat,T}$. This critical value is estimated by considering water activity in non-ideal solutions, applying the Pitzer model to account for ion-specific interactions at the concentrations of interest [97].

In the poromechanical approach by Flatt et al. [109] mirabilite is considered to be uniformly distributed into the porous microstructure of the sample. Considering S_c the volume fraction of the pore space filled with crystals and it is obtained as follows:

$$S_{c,i} = \frac{\bar{\nu}_T}{\bar{\nu}_M}\left[1 - \left(1 - \bar{\nu}_T \frac{c_{Na_2SO_4}}{M_T}\right)^i\right] \quad (2)$$

Where $\bar{\nu}_T$, M_T, $c_{Na_2SO_4}$ represent respectively, the molar volume of thenardite (53.3 $cm^3 \cdot mol^{-1}$); its molar mass of thenardite (142.04 $g \cdot mol^{-1}$); and the sodium sulfate concentration in the used solution. S_c varies between 0 and 1, reflecting the progressive filling of the porous microstructure with sodium sulfate.

By using a representative control volume as reference, the average stress, intended such as the macroscopic tensile stress (σ^*) is represented by:

$$\sigma^* = \sigma_r b S_c \quad (3)$$

where b is the Biot coefficient and σ_r denotes the radial compressive stress (assumed to be equal to ΔPc, Eq. (1)).

Fig. 6 presents a parametric analysis of the variation of S_c with increasing number of cycles for solutions with different sodium sulfate concentrations (2%, 4%, 6%, and 8%). As expected, the higher the salt concentration, the fewer cycles are required for S_c to approach a value of 1.

According to Flatt et al. [109], the critical stress (σ_C^*) for a given material is estimated as follows:

$$\sigma_C^* = \frac{\sigma_T}{\sqrt{3(1-2\nu)}} \quad (4)$$

This analytical formula defines the stress threshold beyond which failure is expected to occur, where ν is the Poisson's ratio and σ_T is the experimentally determined tensile strength [109,125,126].

For the purpose of the present work, focused on materials with a dominant fraction of large pores, it may be useful to introduce a refinement aimed at capturing the different contribution of pore classes to the damage process. To this end, a porosity activation factor α is introduced. This factor, estimated by MIP test, represents the fraction of the total porosity that is considered mechanically active in the development of crystallisation pressure of sodium sulfate [77,112–118]. Accordingly, the crystallized pore volume fraction S_c in the original formulation is replaced by an effective value $S_{c,\,eff}$

$$S_{c,\,eff} = \alpha \cdot S_c \quad (5)$$

where $\alpha \in [0,1]$ depends on the specific material's porosimetric profile (0 for systems in which porosity is distributed within a non critical pore size range for salt crystallisation; 1 for systems in which all porosity falls within the critical pore size range for the salt crystallisation phenomenon). This adjustment allows the model to reflect the microstructural constraints that influence damage development in porous systems with heterogeneous structures or a predominance of larger pores.

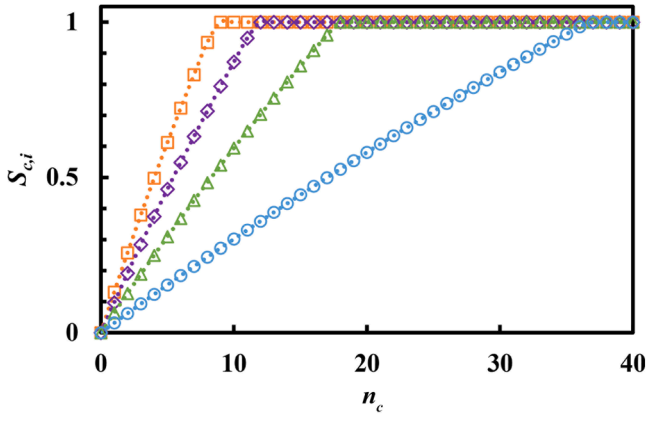

Fig. 6. S_c variation vs n_c. Sodium sulfate concentration equal to 2% (°), 4% (△), 6% (⋄), and 8% (□); $b = 0.7$; $T = 20$ °C.

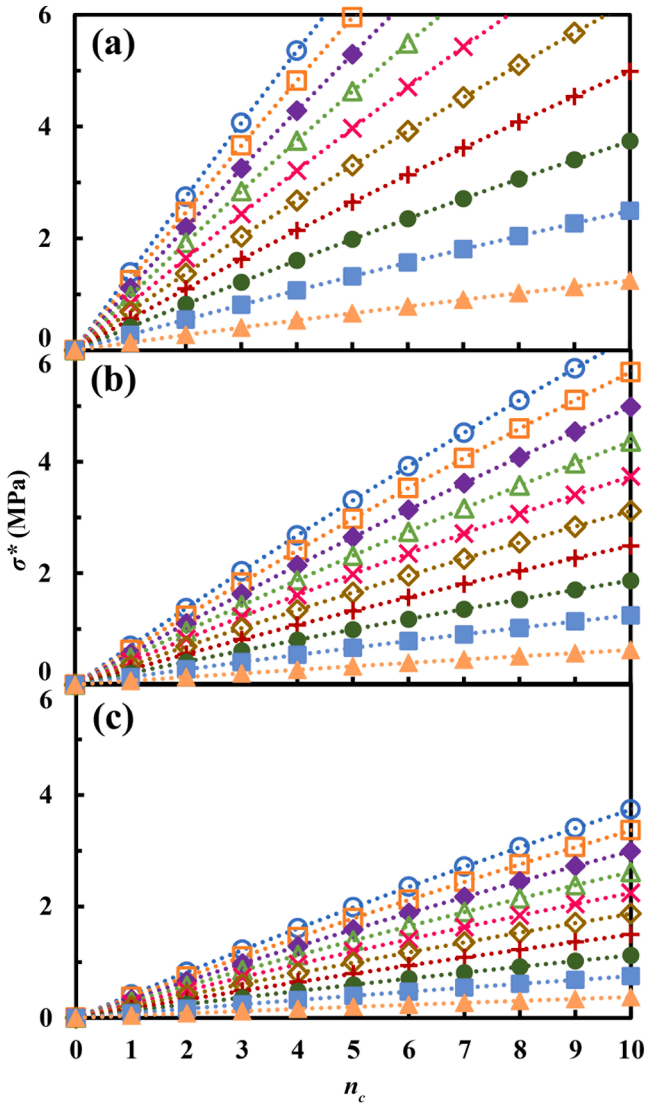

Fig. 7. Variation of σ^* vs n_c. Calculations are performed for diverse values of the Biot coefficient (° 1; □ 0.9; ◆ 0.8; △ 0.7; × 0.6; ⋄ 0.5; + 0.4; ● 0.3; ■ 0.2; ▲ 0.1) and α equal to 1 (a), 0.5 (b) and 0.3 (c).

Fig. 7 presents a parametric analysis in which the Biot coefficient b varies from 0.1 to 1, α assumes values of 1, 0.5, and 0.3.

It can be observed that, as b increases, higher internal stresses develop within the material. Similarly, as α increases, the resulting stress values increases. These trends are consistent with the initial assumptions and align with findings reported in the literature regarding the correlation between critical porosity and macroscopic effects [127]. In this work, the values adopted for the b coefficient range from 0.6 to 0.8. They were not derived from direct experimental calibration but were selected based on a critical analysis of the literature regarding porous and heterogeneous geomaterials [128,129]. Moreover, considering the values of tensile strength (minimum and maximum experimentally acquired, Table 1), ν (0.45), critical porosity (by MIP tests, α equal to 0.30, 0.32 and 0.34 respectively for A, B and C systems), for the materials investigated in this study, Fig. 8 presents the results of the modelling. Based on the adopted assumptions, the onset cycle of material degradation is identified as the point at which σ^* exceeds the σ_C^* of the material (this point graphically corresponds to the intersection between the calculated stress curve and the tensile strength threshold). Filled symbols represent the point at which at least 50% of the samples within a given experimental series exhibit a loss of mass relative to their initial weight

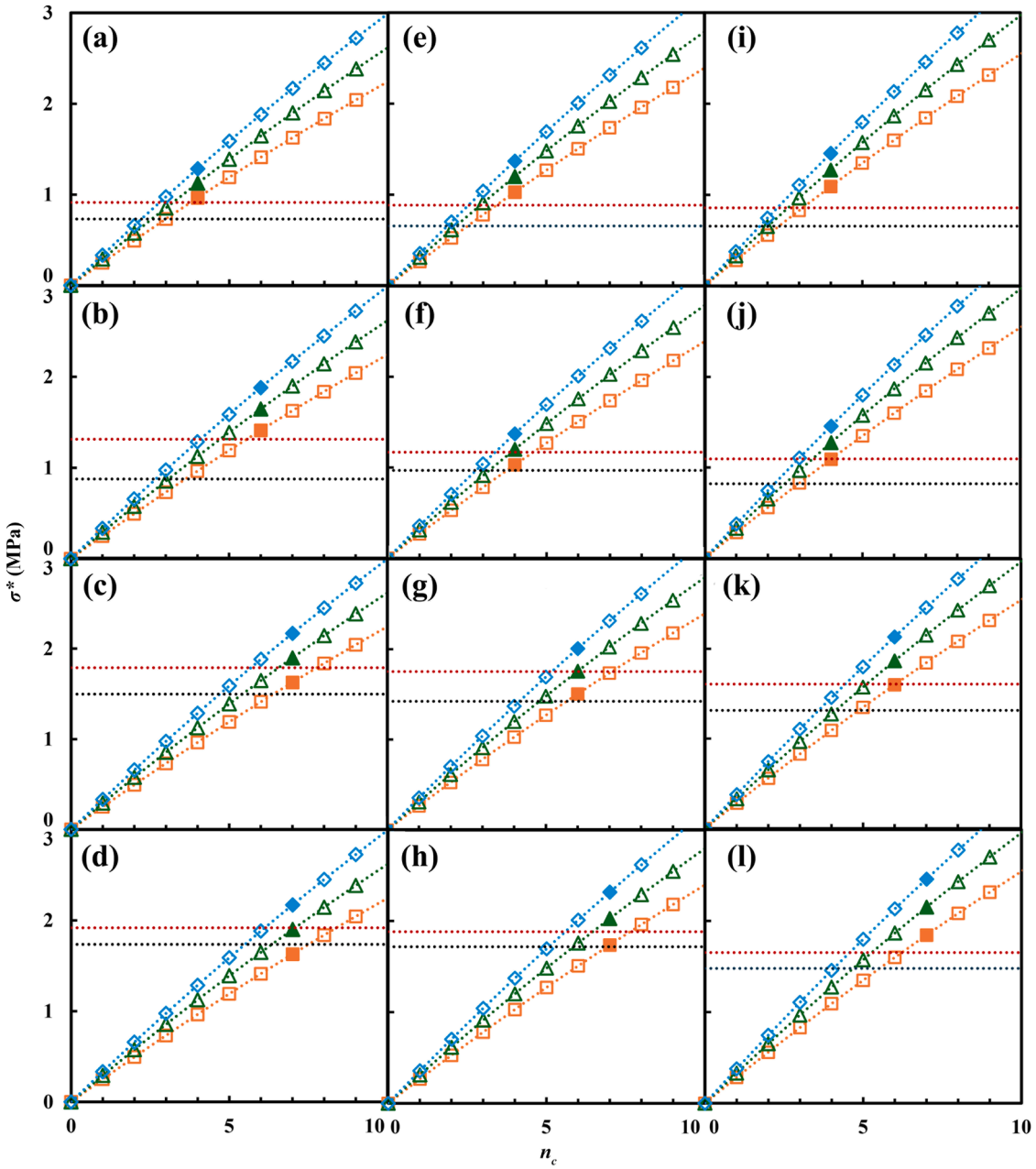

Fig. 8. σ^* calculations and σ_c^* threshold. Solid markers correspond to the experimental cycle at which at least 50% of samples have lost mass compared to their initial dry weight [109]. $T = 293.15$ K; solution concentration: 6.1% (w/w). Biot coefficient is 0.6 (□), 0.7 (△) and 0.8 (◇). The columns show the heat treatments applied to the three different systems: (a) A, 450 °C; (b) A, 500 °C; (c) A, 550 °C; (d) A, 600 °C; (e) B, 450 °C; (f) B, 500 °C; (g) B, 550 °C; (h) B, 600 °C; (i) C, 450 °C; (j) C, 500 °C; (k) C, 550 °C; (l) C, 600 °C.

(condition which is assumed to be the beginning of salt crystallisation-induced degradation) [109].

The comparison between experimental data and numerical simulations highlights the model's ability to accurately capture the initial degradation cycle for the different estimated Biot coefficients, thereby enabling an effective prediction of the phenomenon's progression over time.

Porosity is confirmed to be a microstructural parameter of significant influence on the behavior of materials subjected to salt crystallisation. In particular, samples with a higher pore volume fraction tend to exhibit mass loss after fewer cycles compared to less porous materials. This experimental evidence is not solely attributable to an increase in total porosity, but is closely related to a greater presence of pores within the critical size range for the onset of crystallisation and the associated pressures [130]. The corrective factor represents the fraction of the total porosity that falls within the critical range identified in this study, that is, the portion actively involved in the development of potentially damaging crystallisation pressures.

The importance of introducing a parameter representative of the critical porosity is shown in Fig. 9a, b, where the experimental data, expressed as the number of cycles at which at least 50% of the samples exhibited mass loss relative to their initial value (n_{c_exp}), are first compared with the model predictions (n_{c_mod}) using the specific α parameter for each sample (Fig. 9a), and then with model predictions assuming that the entire porosity corresponds to the critical porosity (Fig. 9b). In both cases, $b = 0.7$. As highlighted, the calculated values closely approximate the experimental results when the approach considering the critical porosity is adopted (Fig. 9a).

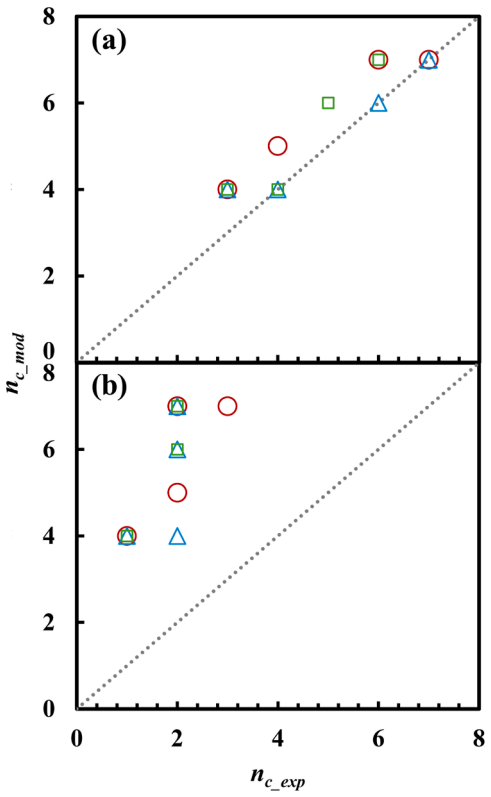

Fig. 9. Comparison between experimental data (n_{c_exp}) and model predictions (n_{c_mod}) for the number of cycles corresponding to 50% mass loss: (a) using the specific critical porosity parameter α for each sample; (b) assuming total porosity as critical. In both cases, $b = 0.7$. A better agreement is observed when the critical porosity is explicitly considered using α.

The results obtained confirm the validity of the adopted modelling approach and strengthen the effectiveness of a straightforward calculation procedure in order to predict material resistance to salt crystallisation cycles. The development of reliable modelling tools represents an important step toward optimizing raw material mix-design processes and thermal stabilization treatments, enabling improvements in material resistance and, consequently, an extension of its service life.

4. Conclusions

In this work, clay-based materials incorporating recycled aggregates were investigated to support circular economy principles and promote sustainable production and construction processes. Three different mix designs were developed by varying the proportions of clay and recycled aggregates. To improve surface strength and durability, the materials were stabilized through low-temperature thermal treatments at 450, 500, 550, and 600 °C for 10 min. The choice to focus on short treatment durations is driven by sustainability considerations. Prolonging the thermal exposure significantly increases energy consumption, which could undermine the environmental advantage of low-temperature stabilization. From a practical perspective, brief treatments are more compatible with real-world constraints, especially in on-site applications. XRD analysis revealed the onset of mineralogical transformations correlated with increasing treatment temperatures. Tensile strength values ranged between 0.460 ÷ 1 MPa, 0.423 ÷ 0.985 MPa, and 0.415 ÷ 0.858 MPa for systems A, B, and C, respectively, with the average porosity ranging from 20.11 ÷ 22.76%, 22.59 ÷ 25.35%, and 26.70 ÷ 28.55%, confirming a direct correlation between porosity and the amount of recycled aggregate.

Total immersion tests demonstrated effective water resistance across all systems, confirming the success of thermal stabilization. The different formulations were then subjected to sodium sulfate salt crystallisation cycles. The onset of degradation was defined as the cycle at which at least 50% of the specimens exhibited a measurable weight loss relative to their initial dry mass. A progressively higher susceptibility to salt-induced damage was observed from system A to C, with system C being the most affected. This depends on both the mix design and the thermal treatment temperatures.

A chemo-mechanical model was applied to predict the onset of damage based on the exceedance of the material's tensile strength. The modelling approach was refined by introducing a parameter representing the critical pore fraction α, i.e., the portion of porosity most actively involved in salt crystallisation. The model predictions showed excellent agreement with experimental results, confirming the reliability of the proposed approach. Although certain aspects, such as the dispersion of experimental data and the complexity involved in determining the Biot coefficient (both required as model inputs), represent limitations of this approach, the parametric analyses have shown that the results remain reliable across a wide range of input variations. The model can therefore be understood as a tool for both estimating and validating experimentally acquired and derived data. Beyond the interpretation of experimental results, the present study demonstrates the application of the analytical model as an initial step toward the development of a predictive framework for the design of sustainable earthen materials with recycled aggregates. The generalization of the model could also involve the prediction of crystallization-induced damage from different salt types, which would require modifying the analytical procedure to account for salt-specific parameters (such as the critical pore fraction α, crystallization pressure, and solubility characteristics) alongside a dedicated and extensive experimental campaign.

Overall, the stabilized clay-based materials studied in this work demonstrate good resistance to sodium sulfate crystallization damage and appear promising for improving the sustainability of construction materials. A key advantage is the short thermal treatment time, which qualitatively reduces energy consumption. This makes the approach particularly attractive for sustainable construction projects, temporary structures, and applications in regions with limited industrial infrastructure. In future work, it will be of interest to investigate the effects of varying thermal treatment times, temperatures, and application methods (both industrial and on-site). In this regard, an important step forward will be represented by a rigorous, quantitative comparison of energy consumption and environmental impact between different stabilization methods, which will require a dedicated study based on Life Cycle Assessment (LCA) protocols.

Furthermore, it will be relevant to evaluate the full degradation kinetics up to the point of complete disintegration or decohesion of the material by extending the accelerated aging tests over a higher number of crystallization cycles. For this reason, the present work represents a necessary preliminary step focused on verifying the material's effectiveness in resisting salt crystallization.

CRediT authorship contribution statement

Marta Cappai: Writing – review & editing, Writing – original draft, Visualization, Validation, Software, Methodology, Investigation, Formal analysis, Data curation, Conceptualization. **Giorgio Pia:** Writing – review & editing, Writing – original draft, Visualization, Validation, Supervision, Software, Resources, Project administration, Methodology, Investigation, Funding acquisition, Formal analysis, Data curation, Conceptualization.

Declaration of competing interest

The authors declare that they have no known competing financial interests or personal relationships that could have appeared to influence the work reported in this paper.

Acknowledgements

The authors are grateful to University of Cagliari and Materialia Association. R.E.R. s.r.l. is gratefully acknowledged for providing the raw materials essential to the development of this work.

Data availability

Data will be made available on request.

References

[1] United Nations Environment Programme, Global status report for buildings and construction. Beyond foundations: mainstreaming sustainable solutions to cut emissions from the buildings sector, (2024). 10.59117/20.500.11822/45095.
[2] United Nations Environment Programme, building materials and the climate: constructing a new future, (2023).
[3] EUROPEAN COMMISSION, stepping up Europe's 2030 climate ambition. Investing in a climate-neutral future for the benefit of our people. COM(2020) 562 final, (2020). https://eur-lex.europa.eu/legal-content/EN/TXT/?uri=celex:52020DC0562 (accessed March 5, 2025).
[4] S. Wolf, J. Teitge, J. Mielke, F. Schütze, C. Jaeger, The European green deal–more than climate neutrality, Intereconomics 56 (2021) 99–107, https://doi.org/10.1007/s10272-021-0963-z.
[5] Supriya, R. Chaudhury, U. Sharma, P.C. Thapliyal, L.P. Singh, Low-CO2 emission strategies to achieve net zero target in cement sector, J. Clean. Prod. 417 (2023), https://doi.org/10.1016/j.jclepro.2023.137466.
[6] R.M. Andrew, Global CO2 emissions from cement production, 1928-2018, Earth Syst. Sci. Data 11 (2019) 1675–1710, https://doi.org/10.5194/essd-11-1675-2019.
[7] U.N.E. Programme, 2022 GLOBAL status for buildings an construction, 2022.
[8] S. Fawzy, A.I. Osman, J. Doran, D.W. Rooney, Strategies for mitigation of climate change: a review, Environ. Chem. Lett. 18 (2020) 2069–2094, https://doi.org/10.1007/s10311-020-01059-w.
[9] S. Barbhuiya, B. Bhusan Das, D. Adak, Roadmap to a net-zero carbon cement sector: strategies, innovations and policy imperatives, J. Environ. Manag. 359 (2024), https://doi.org/10.1016/j.jenvman.2024.121052.
[10] S. Barbhuiya, F. Kanavaris, B.B. Das, M. Idrees, Decarbonising cement and concrete production: strategies, challenges and pathways for sustainable development, J. Build. Eng. 86 (2024), https://doi.org/10.1016/j.jobe.2024.108861.
[11] M. Gernot, Building with earth, Thirdand r, 2013. 10.3362/9781780443959.
[12] R. Rael, Earth Architecture, Princeton, 2009.
[13] H. Schroeder, Sustainable building with earth, 2015. 10.1007/978-3-319-19491-2.
[14] A. Fabbri, J.C. Morel, Earthen materials and constructions. Nonconventional and Vernacular Construction Materials, Elsevier, 2016, pp. 273–299, https://doi.org/10.1016/B978-0-08-100038-0.00010-X.
[15] G.J. Frencham, The performance of earth buildings, 1982.
[16] H. Hugo, H. Guillard, Earth construction: a comprehensive guide, 1994.
[17] L. Ben-Alon, A.R. Rempel, Thermal comfort and passive survivability in earthen buildings, Build. Environ. 238 (2023) 110339, https://doi.org/10.1016/j.buildenv.2023.110339.
[18] M. Hanafi, I. Javed, A. Ekinci, Evaluating the strength, durability and porosity characteristics of alluvial clay stabilized with marble dust as a sustainable binder, Results Eng. 25 (2025), https://doi.org/10.1016/j.rineng.2025.103978.
[19] S.I. Kaitouni, F.Z. Gargab, A. Tabit, M. Mabrouki, N. Lamdouar, A. Jamil, M. Ahachad, A life cycle carbon dioxide equivalent emissions assessment of zero carbon building in hot semi-arid climate region: case study, Results Eng. 23 (2024), https://doi.org/10.1016/j.rineng.2024.102589.
[20] A.A. Firoozi, A.A. Firoozi, D.O. Oyejobi, S. Avudaiappan, E.S. Flores, Emerging trends in sustainable building materials: technological innovations, enhanced performance, and future directions, Results Eng. 24 (2024), https://doi.org/10.1016/j.rineng.2024.103521.
[21] H.A. Vaghefi-Rezaee, H. Sarvari, S. Khademi-Adel, D.J. Edwards, C.J. Roberts, A scientometric review and analysis of studies on the barriers and challenges of sustainable construction, Buildings 14 (2024), https://doi.org/10.3390/buildings14113432.
[22] P. De Joanna, The earthen architecture and standards requirements, SMC 1 (2014) 70–74.
[23] Y. Zhang, S. Jiang, D. Quan, K. Fang, B. Wang, Z. Ma, Properties of sustainable earth construction materials: a state-of-the-art review, Sustainability 16 (2024), https://doi.org/10.3390/su16020670.
[24] M.S. Zami, A. Lee, Economic benefits of contemporary earth construction in low-cost urban housing–state-of-the-art review, J. Build. Apprais. 5 (2010) 259–271, https://doi.org/10.1057/jba.2009.32.
[25] R. Charles, Barriers and strategies for sustainable building practices in small-scale construction: insights from literature and industry stakeholders, 2025. https://www.researchgate.net/publication/389178523.
[26] V. Mora-Ruiz, J. Soto-Paz, S. Attia, C. Mejía-Parada, Sustainable earthen construction: a meta-analytical review of environmental, mechanical, and thermal performance, Buildings 15 (2025) 918, https://doi.org/10.3390/buildings15060918.
[27] M. La Noce, A. Lo Faro, G. Sciuto, Clay-based products sustainable development: some applications, Sustainability 13 (2021) 1–28, https://doi.org/10.3390/su13031364.
[28] G. Giuffrida, L. Dipasquale, R.M. Pulselli, R. Caponetto, Compared environmental lifecycle performances of earth-based walls to drive building envelope design, Sustainability 16 (2024), https://doi.org/10.3390/su16041367.
[29] P. Nshimiyimana, A. Messan, L. Courard, Physico-mechanical and hygro-thermal properties of compressed earth blocks stabilized with industrial and agro by-product binders, Materials 13 (2020), https://doi.org/10.3390/ma13173769.
[30] M. Lachheb, N. Youssef, Z. Younsi, A comprehensive review of the improvement of the thermal and mechanical properties of unfired clay bricks by incorporating waste materials, Buildings 13 (2023), https://doi.org/10.3390/buildings13092314.
[31] Y. Nasr, H. El Zakhem, A.E.A. Hamami, M. El Bachawati, R. Belarbi, Comprehensive review of innovative materials for sustainable buildings' Energy performance, Energies 16 (2023), https://doi.org/10.3390/en16217440.
[32] J.C. Morel, R. Charef, E. Hamard, A. Fabbri, C. Beckett, Q.B. Bui, Earth as construction material in the circular economy context: practitioner perspectives on barriers to overcome, Philos. Trans. R. Soc. B Biol. Sci. 376 (2021), https://doi.org/10.1098/rstb.2020.0182.
[33] K.A. Heathcote, Durability of earthwall buildings, Constr. Build. Mater. 9 (1995) 185–189, https://doi.org/10.1016/0950-0618(95)00035-E.
[34] E. Quagliarini, M. D'Orazio, S. Lenci, The Properties and Durability of Adobe Earth-Based Masonry Blocks, Elsevier Ltd, 2014, https://doi.org/10.1016/B978-1-78242-305-8.00016-4.
[35] C.T.S. Beckett, P.A. Jaquin, J.C. Morel, Weathering the storm: a framework to assess the resistance of earthen structures to water damage, Constr. Build. Mater. 242 (2020) 118098, https://doi.org/10.1016/j.conbuildmat.2020.118098.
[36] M. Cappai, F. Delogu, D. Pozzi-Escot, G.P. Neyra, P. Meloni, G. Pia, Degradation phenomena of Templo Pintado painted plasters, Constr. Build. Mater. 392 (2023) 131839, https://doi.org/10.1016/j.conbuildmat.2023.131839.
[37] M. Cappai, L. Casnedi, G. Carcangiu, F. Delogu, D. Pozzi-escot, G. Pacheco, G. Pia, P. Meloni, Weathering of earth-painted surfaces : environmental monitoring and artificial aging, Constr. Build. Mater. 344 (2022) 128193, https://doi.org/10.1016/j.conbuildmat.2022.128193.
[38] K.K.G.K.D. Kariyawasam, C. Jayasinghe, Cement stabilized rammed earth as a sustainable construction material, Constr. Build. Mater. 105 (2016) 519–527, https://doi.org/10.1016/j.conbuildmat.2015.12.189.
[39] H. Van Damme, H. Houben, Earth concrete. Stabilization revisited, Cem. Concr. Res. 114 (2016) 90–102, https://doi.org/10.1016/j.cemconres.2017.02.035.
[40] M.I. Gomes, P. Faria, T.D. Gonçalves, Earth-based mortars for repair and protection of rammed earth walls. Stabilization with mineral binders and fibers, J. Clean. Prod. 172 (2018) 2401–2414, https://doi.org/10.1016/j.jclepro.2017.11.170.
[41] S. Real, J.A. Bogas, R. Cruz, M.G. Gomes, Eco-recycled cement's effect on the microstructure and hygroscopic behaviour of compressed stabilised earth blocks, J. Build. Eng. 95 (2024), https://doi.org/10.1016/j.jobe.2024.110227.
[42] A. Koutous, E. Hilali, Compression stress-strain curve of rammed earth: measuring and modelling, Results Eng. 18 (2023), https://doi.org/10.1016/j.rineng.2023.101012.
[43] M.D.R. Veiga, A. Fragata, A.L. Velosa, A.C. Magalhães, G. Margalha, Lime-based mortars: viability for use as substitution renders in historical buildings, Int. J. Archit. Herit. 4 (2010) 177–195, https://doi.org/10.1080/15583050902914678.
[44] B. Taallah, A. Guettala, The mechanical and physical properties of compressed earth block stabilized with lime and filled with untreated and alkali-treated date palm fibers, Constr. Build. Mater. 104 (2016) 52–62, https://doi.org/10.1016/j.conbuildmat.2015.12.007.
[45] S.N. Malkanthi, N. Balthazaar, A.A.D.A.J. Perera, Lime stabilization for compressed stabilized earth blocks with reduced clay and silt, Case Stud. Constr. Mater. 12 (2020), https://doi.org/10.1016/j.cscm.2019.e00326.
[46] A.W. Bruno, L.M. Lalicata, R. Abdallah, A. Lagazzo, S. Arris-Roucan, F. McGregor, C. Perlot, D. Gallipoli, Synergic effect of hydrated lime and guar gum stabilisation on the mechanical, thermal and hygroscopic behaviour of a Ligurian earth material, Constr. Build. Mater. 439 (2024), https://doi.org/10.1016/j.conbuildmat.2024.137258.
[47] M. Cappai, R. Shoukat, L. Pilia, R. Ricciu, D. Lai, G. Marongiu, G. Pia, Thermal properties of eco-friendly earthen materials stabilized with bio-based polymers: experimental data and modeling procedure for improving mix-design, Materials 17 (2024) 1035, https://doi.org/10.3390/ma17051035.
[48] N. Sohaib, M.S. Faiz, G. Sana, Use of acrylic polymer for stabilization of clayey soil, Int. J. Sci. Eng. Res. 9 (2018) 433–438.
[49] S.S. Park, J.S. Lee, K.B. Yoon, S.W. Woo, D.E. Lee, Application of an acrylic polymer and epoxy emulsion to red clay and sand, Polymers 13 (2021) 1–15, https://doi.org/10.3390/polym13193410.
[50] P. Melià, G. Ruggieri, S. Sabbadini, G. Dotelli, Environmental impacts of natural and conventional building materials: a case study on earth plasters, J. Clean. Prod. 80 (2014) 179–186, https://doi.org/10.1016/j.jclepro.2014.05.073.
[51] A.E. Losini, A.C. Grillet, M. Bellotto, M. Woloszyn, G. Dotelli, Natural additives and biopolymers for raw earth construction stabilization – a review, Constr. Build. Mater. 304 (2021) 124507, https://doi.org/10.1016/j.conbuildmat.2021.124507.
[52] T. Sesay, Y. Xie, Y. Chen, J. Xue, Bio-based stabilization of natural soil for rammed Earth construction: a review on mechanical and water durability performance, Polymers 17 (2025), https://doi.org/10.3390/polym17091170.

[53] R. Shoukat, M. Cappai, G. Pia, T. Kubaszek, R. Ricciu, Ł. Kolek, L. Pilia, Thermal conductivity of sustainable earthen materials stabilized by natural and bio-based polymers: an experimental and statistical analysis, Energies 18 (2025), https://doi.org/10.3390/en18123144.
[54] A. Vissac, A. Bourgès, D. Gandreau, R. Anger, L. Fontaine, Argiles & biopolymères, CRAterre é, 2017.
[55] S. Muguda, S.J. Booth, P.N. Hughes, C.E. Augarde, C. Perlot, A.W. Bruno, D. Gallipoli, Mechanical properties of biopolymer-stabilised soil-based construction materials, Geotech. Lett. 7 (2017) 309–314, https://doi.org/10.1680/jgele.17.00081.
[56] A. Soldo, M. Miletic, Durability against wetting-drying cycles of sustainable biopolymer-treated soil, Polymers 14 (2022) 1–14, https://doi.org/10.3390/polym14194247.
[57] N. Latifi, S. Horpibulsuk, C.L. Meehan, M.Z.A. Majid, M.M. Tahir, E.T. Mohamad, Improvement of problematic soils with biopolymer–an environmentally friendly soil stabilizer, J. Mater. Civ. Eng. 29 (2017) 1–11, https://doi.org/10.1061/(asce)mt.1943-5533.0001706.
[58] B. Ilman, A.P. Balkis, Sustainable biopolymer stabilized earthen: utilization of chitosan biopolymer on mechanical, durability, and microstructural properties, J. Build. Eng. 76 (2023), https://doi.org/10.1016/j.jobe.2023.107220.
[59] I. Chang, J. Im, A.K. Prasidhi, G.C. Cho, Effects of Xanthan gum biopolymer on soil strengthening, Constr. Build. Mater. 74 (2015) 65–72, https://doi.org/10.1016/j.conbuildmat.2014.10.026.
[60] S. Muguda, G. Lucas, P.N. Hughes, C.E. Augarde, C. Perlot, A.W. Bruno, D. Gallipoli, Durability and hygroscopic behaviour of biopolymer stabilised earthen construction materials, Constr. Build. Mater. 259 (2020) 119725, https://doi.org/10.1016/j.conbuildmat.2020.119725.
[61] S. Muguda, S.J. Booth, P.N. Hughes, C.E. Augarde, C. Perlot, A.W. Bruno, D. Gallipoli, Preliminary study on use of biopolymers in earthen construction, in: Proceedings of the 7th International Conference on Unsaturated Soils, 2018.
[62] J. Plank, Applications of biopolymers and other biotechnological products in building materials, Appl. Microbiol. Biotechnol. 66 (2004) 1–9, https://doi.org/10.1007/s00253-004-1714-3.
[63] R. Shoukat, M. Cappai, L. Pilia, G. Pia, Rice starch chemistry, functional properties, and industrial applications: a review, Polymers 17 (2025) 110, https://doi.org/10.3390/polym17010110.
[64] R. Shoukat, M. Cappai, G. Pia, L. Pilia, An updated review: opuntia ficus indica (OFI) Chemistry and its diverse applications, Appl. Sci. 13 (2023) 7724, https://doi.org/10.3390/app13137724.
[65] E. Bernat-Maso, L. Gil, M.J. Lis, E. Teneva, Soil biostabilisation and interaction with compaction processes for earthen engineering structures production, Mater. Constr. 71 (2021), https://doi.org/10.3989/MC.2021.00221.
[66] E. Bernat-Maso, L. Gil, C. Escrig, J. Barbé, P. Cortés, Effect of sporosarcina pasteurii on the strength properties of compressed earth specimens, Mater. Constr. 68 (2018), https://doi.org/10.3989/mc.2018.12316.
[67] A. Bras, H. Mohammed, A. Romano, I. Nakouti, Biomineralisation to increase earth infrastructure resilience, Materials 15 (2022), https://doi.org/10.3390/ma15072490.
[68] H. Niroumand, M.F.M. Zain, M. Jamil, The role of nanotechnology in rammed earth walls and earth buildings, Procedia Soc. Behav. Sci. 89 (2013) 243–247, https://doi.org/10.1016/j.sbspro.2013.08.842.
[69] H. Niroumand, M.F.M. Zain, S.N. Alhosseini, The influence of nano-clays on compressive strength of earth bricks as sustainable materials, Procedia Soc. Behav. Sci. 89 (2013) 862–865, https://doi.org/10.1016/j.sbspro.2013.08.945.
[70] J. Calabria A, W.L. Vasconcelos, D.J. Daniel, R. Chater, D. McPhail, A. R. Boccaccini, Synthesis of sol-gel titania bactericide coatings on adobe brick, Constr. Build. Mater. 24 (2010) 384–389, https://doi.org/10.1016/j.conbuildmat.2009.08.020.
[71] T.P. Ngo, Q.B. Bui, N.T. Nguyen, T. Le, V.T.A. Phan, Application of nanotechnology for earth materials: an exploratory study with graphene-based nanosheets, Constr. Build. Mater. 324 (2022), https://doi.org/10.1016/j.conbuildmat.2022.126677.
[72] B. Akturk, H. Gulen, B.C. Keskin, F. Akipek, T. Yazar, Investigating the possible bio-stabilization of rammed Earth through microorganisms, in: Proceedings of the 4th International Congress on Materials & Structural Stability, Rabat, 2023. https://www.researchgate.net/publication/369339310.
[73] A. Karozou, E. Pavlidou, M. Stefanidou, Enhancing properties of clay mortars using nano-additives, Solid State Phenom. 286 (2019) 145–155, https://doi.org/10.4028/www.scientific.net/SSP.286.145.
[74] A.S. Rieppi Godoy, L.E. Peisino, G. Rolón, B.B. Raggiotti, Firing the wall: a novel way to protect earth buildings, Constr. Build. Mater. 445 (2024), https://doi.org/10.1016/j.conbuildmat.2024.137878.
[75] M. Cappai, G. Pia, Sustainable earthen plasters: surface resistance enhancement via thermal treatments, J. Build. Eng. 108 (2025), https://doi.org/10.1016/j.jobe.2025.112867.
[76] C. Atzeni, G. Pia, U. Sanna, N. Spanu, Surface wear resistance of chemically or thermally stabilized earth-based materials, Mater. Struct./Mater. Constr. 41 (2008) 751–758, https://doi.org/10.1617/s11527-007-9278-1.
[77] D. Benavente, M.A.G. del Cura, R. Fort, S. Ordónez, Durability estimation of porous building stones from pore structure and strength, Eng. Geol. 74 (2004) 113–127, https://doi.org/10.1016/j.enggeo.2004.03.005.
[78] Á. Rabat, M. Cano, R. Tomás, Effect of water saturation on strength and deformability of building calcarenite stones: correlations with their physical properties, Constr. Build. Mater. 232 (2020) 117259, https://doi.org/10.1016/j.conbuildmat.2019.117259.
[79] R. Kilian, L. Borgatta, E. Wendler, Investigation of the deterioration mechanisms induced by moisture and soluble salts in the necropolis of Porta Nocera, Pompeii (Italy), Herit. Sci. 11 (2023) 1–21, https://doi.org/10.1186/s40494-023-00900-z.
[80] J. Yue, Y. Li, Z. Luo, X. Huang, Q. Kong, Z. Wang, Study on deterioration law and mechanism of gray brick due to salt crystallization, Materials 15 (2022), https://doi.org/10.3390/ma15082936.
[81] M. Cappai, M. Casti, G. Pia, Salt crystallization in limestone: materials decay and chemomechanical approach, Materials 17 (2024), https://doi.org/10.3390/ma17163986.
[82] S. Scrivano, L. Gaggero, An experimental investigation into the salt-weathering susceptibility of building limestones, Rock Mech. Rock Eng. 53 (2020) 5329–5343, https://doi.org/10.1007/s00603-020-02208-x.
[83] H. Yang, C. Chen, J. Ni, S. Karekal, A hyperspectral evaluation approach for quantifying salt-induced weathering of sandstone, Sci. Total Environ. 885 (2023) 163886, https://doi.org/10.1016/j.scitotenv.2023.163886.
[84] Q. xiang Xiong, L. yu Tong, J. kai Huang, J. Yang, Q. Feng Liu, Salt crystallization in porous materials: a quasi-local transport model for evaluating pore filling process, Constr. Build. Mater. 462 (2025), https://doi.org/10.1016/j.conbuildmat.2025.139904.
[85] D.E. Valdez Madrid, N. De Belie, V. Cnudde, Performance of cement-lime mortars against salt crystallization using experimental accelerated weathering tests, Cem. Concr. Compos. (2025) 106196, https://doi.org/10.1016/j.cemconcomp.2025.106196.
[86] C. Cardell, F. Delalieux, K. Roumpopoulos, A. Moropoulou, F. Auger, R. Van Grieken, Salt-induced decay in calcareous stone monuments and buildings in a marine environment in SW France, Constr. Build. Mater. 17 (2003) 165–179, https://doi.org/10.1016/S0950-0618(02)00104-6.
[87] E.M. Winkler, Moisture and salts in stone. Stone in Architecture, Springer, Berlin, Heidelberg, 1997, pp. 142–186, https://doi.org/10.1007/978-3-662-10070-7_6.
[88] S. Yun-xia, C. Wen-wu, K. Jing, D.U. Wei-fei, Effect of salts on earthen materials deterioration after humidity cycling, J. Cent. South Univ. 24 (2017) 796–806, https://doi.org/10.1007/s11771-017-3482-0.
[89] A.E. Charola, Salts in the deterioration of porous materials : an overview, J. Am. Inst. Conserv. 39 (2000) 327–343.
[90] R.M. Espinosa-Marzal, G.W. Scherer, Mechanisms of damage by salt, Geol. Soc. Spec. Publ. 331 (2010) 61–77, https://doi.org/10.1144/SP331.5.
[91] C.T. Oguchi, S. Yu, A review of theoretical salt weathering studies for stone heritage, Prog. Earth Planet. Sci. 8 (2021), https://doi.org/10.1186/s40645-021-00414-x.
[92] A. La Iglesia, V. González, V. López-Acevedo, C. Viedma, Salt crystallization in porous construction materials I estimation of crystallization pressure, J. Cryst. Growth 177 (1997) 111–118, https://doi.org/10.1016/S0022-0248(96)01072-X.
[93] R.J. Flatt, N.A. Mohamed, F. Caruso, H. Derluyn, J. Desarnaud, B. Lubelli, R. M. Espinosa-marzal, L. Pel, C. Rodriguez-navarro, G.W. Scherer, N. Shahidzadeh, M. Steiger, Predicting salt damage in practice: a theoretical insight into laboratory tests, RILEM Tech. Lett. 2 (2017) 108–118, https://doi.org/10.21809/rilemtechlett.2017.41.
[94] M. Cappai, M. Casti, G. Pia, Monitoring and preservation of stone cultural heritage using a fuzzy model for predicting salt crystallisation damage, Sci. Rep. 14 (2024) 22671, https://doi.org/10.1038/s41598-024-73192-3.
[95] J.M.P.Q. Delgado, A.S. Guimarães, V.P. De Freitas, I. Antepara, V. Kočí, R. Černý, Salt damage and rising damp treatment in building structures, Adv. Mater. Sci. Eng. 2016 (2016), https://doi.org/10.1155/2016/1280894.
[96] M. Cappai, U. Sanna, G. Pia, A fuzzy model for studying kinetic decay phenomena in Genna Maria Nuraghe: material properties, environmental data, accelerated ageing, and model calculations, Case Stud. Constr. Mater. 21 (2024), https://doi.org/10.1016/j.cscm.2024.e03513.
[97] M. Steiger, S. Asmussen, Crystallization of sodium sulfate phases in porous materials: the phase diagram Na2SO4-H2O and the generation of stress, Geochim. Cosmochim. Acta 72 (2008) 4291–4306, https://doi.org/10.1016/j.gca.2008.05.053.
[98] M. Angeli, R. Hébert, B. Menéndez, C. David, J.P. Bigas, Influence of temperature and salt concentration on the salt weathering of a sedimentary stone with sodium sulphate, Eng. Geol. 115 (2010) 193–199, https://doi.org/10.1016/j.enggeo.2009.06.001.
[99] C. Rodriguez-Navarro, E. Doehne, E. Sebastian, How does sodium sulfate crystallize? Implications for the decay and testing of building materials, Cem. Concr. Res. 30 (2000) 1527–1534, https://doi.org/10.1016/S0008-8846(00)00381-1.
[100] P. Lopez-Arce, E. Doehne, Kinetics of sodium sulfate efflorescence as observed by humidity cycling with ESEM, in: Proceedings of the International Conference on Heritage, Weathering and Conservation 1, HWC, 2006, pp. 285–291, 2006.
[101] R.M.E. Marzal, G.W. Scherer, Crystallization of sodium sulfate salts in limestone, Environ. Geol. 56 (2008) 605–621, https://doi.org/10.1007/s00254-008-1441-7.
[102] N. Tsui, R.J. Flatt, G.W. Scherer, Crystallization damage by sodium sulfate, J. Cult. Herit. 4 (2003) 109–115, https://doi.org/10.1016/S1296-2074(03)00022-0.
[103] S. Chatterji, A.D. Jensen, Efflorescence and Breakdown of Building Materials, Nordic Concrete Federation, 1989.
[104] L. Germinario, C.T. Oguchi, Underground salt weathering of heritage stone: lithological and environmental constraints on the formation of sulfate efflorescences and crusts, J. Cult. Herit. 49 (2021) 85–93, https://doi.org/10.1016/j.culher.2021.02.011.
[105] X. Zhang, X. Wu, S. Ling, Y. Cao, Efflorescence, subflorescence, and crust weathering characteristics of sandstone in Nankan Grotto, China: insights into

petrography and environment constraints, Herit. Sci. 12 (2024) 1–16, https://doi.org/10.1186/s40494-024-01371-6.
[106] Q. Sun, Z. Dong, H. Jia, Decay of sandstone subjected to a combined action of repeated freezing–thawing and salt crystallization, Bull. Eng. Geol. Environ. 78 (2019) 5951–5964, https://doi.org/10.1007/s10064-019-01490-6.
[107] R.M.E. Marzal, L. Franke, G. Deckelmann, Predicting efflorescence and subflorescences of salts, Mater. Res. Soc. Symp. Proc. 1047 (2008) 105–114, https://doi.org/10.1557/proc-1047-y04-03.
[108] R.J. Flatt, Salt damage in porous materials : how high supersaturations are generated, J. Cryst. Growth 242 (2002) 435–454.
[109] R.J. Flatt, F. Caruso, A.M.A. Sanchez, G.W. Scherer, Chemo-mechanics of salt damage in stone, Nat. Commun. 5 (2014) 1–5, https://doi.org/10.1038/ncomms5823.
[110] M.C. Gastuche, F. Toussaint, J.J. Fripiat, R. Touilleaux, M. Van Meersche, Study of intermediate stages in the kaolin→ metakaolin transformation, Clay Miner. Bull. 29 (1963) 227–236.
[111] Y.O. Abiodun, O.M. Sadiq, S.O. Adeosun, G.L. Oyekan, Mineralogical properties of kaolin and metakaolin from selected areas in Nigeria and its application to concrete production, West Indian J. Eng. 1 (2019).
[112] K. Zehnder, A. Arnold, Crystal growth in salt efflorescence, 1989.
[113] M. Steiger, Crystal growth in porous materials - II: influence of crystal size on the crystallization pressure, J. Cryst. Growth 282 (2005) 470–481, https://doi.org/10.1016/j.jcrysgro.2005.05.008.
[114] G.W. Scherer, Internal stress and cracking in stone and masonry. Measuring, Monitoring and Modeling Concrete Properties, Springer Netherlands, Dordrecht, 2006, pp. 633–641, https://doi.org/10.1007/978-1-4020-5104-3_77.
[115] S. Ordóñez, R. Fort, M.A. Garcia del Cura, Pore size distribution and the durability of a porous limestone, Q. J. Eng. Geol. 30 (1997) 221–230, https://doi.org/10.1144/GSL.QJEG.1997.030.P3.04.
[116] A.R. Punuru, A.N. Chowdhury, N.P. Kulshreshtha, K.L. Gauri, Control of porosity on durability of limestone at the great sphinx, Egypt, Environ. Geol. Water Sci. 15 (1990) 225–232, https://doi.org/10.1007/BF01706414.
[117] R. Rossi-Manaresi, A. Tucci, Pore structure and the disruptive or cementing effect of salt crystallization in various types of stone, Stud. Conserv. 36 (1991) 53–58, https://doi.org/10.1179/sic.1991.36.1.53.
[118] B.K. Moh'd, R.J. Howarth, C.H. Bland, Rapid prediction of building research establishment limestone durability class from porosity and saturation, Q. J. Eng. Geol. 29 (1996) 285–297, https://doi.org/10.1144/GSL.QJEGH.1996.029.P4.03.
[119] P.M. Nigay, T. Cutard, A. Nzihou, The impact of heat treatment on the microstructure of a clay ceramic and its thermal and mechanical properties, Ceram. Int. 43 (2017) 1747–1754, https://doi.org/10.1016/j.ceramint.2016.10.084.
[120] P. Poullain, M. Barnaure, S. Bonnet, Variability of the mechanical properties of earthen composites, SSRN Electron. J. (2022), https://doi.org/10.2139/ssrn.4159294.
[121] P. Poullain, M. Barnaure, S. Bonnet, Mechanical properties of cob-earth composites: variability and focus on the different calculation methods of Young's modulus, J. Build. Eng. 72 (2023), https://doi.org/10.1016/j.jobe.2023.106622.
[122] M. Barnaure, S. Bonnet, P. Poullain, Earth buildings with local materials: assessing the variability of properties measured using non-destructive methods, Constr. Build. Mater. 281 (2021), https://doi.org/10.1016/j.conbuildmat.2021.122613.
[123] J. Tchiotsop, N. Issaadi, P. Poullain, S. Bonnet, R. Belarbi, Assessment of the natural variability of cob buildings hygric and thermal properties at material scale: influence of plants add-ons, Constr. Build. Mater. 342 (2022), https://doi.org/10.1016/j.conbuildmat.2022.127922.
[124] M. Nasiri Pishvari, M. Salimi, M. Payan, H. Ahmadi, M. Zamanian, R.J. Chenari, Influence of inherent anisotropy on the mechanical properties of normally consolidated clays with a wide range of plasticity indices, Results Eng. 24 (2024), https://doi.org/10.1016/j.rineng.2024.103323.
[125] R.M. Espinosa-Marzal, A. Hamilton, M. McNall, K. Whitaker, G.W. Scherer, The chemomechanics of crystallization during rewetting of limestone impregnated with sodium sulfate, J. Mater. Res. 26 (2011) 1472–1481, https://doi.org/10.1557/jmr.2011.137.
[126] O. Coussy, Deformation and stress from in-pore drying-induced crystallization of salt, J. Mech. Phys. Solids 54 (2006) 1517–1547, https://doi.org/10.1016/j.jmps.2006.03.002.
[127] D. Hübner, E. Rohan, V. Lukeš, M. Stingl, Optimization of the porous material described by the Biot model, Int. J. Solids Struct. 156–157 (2019) 216–233, https://doi.org/10.1016/j.ijsolstr.2018.08.016.
[128] D. Knez, M.A.M. Zamani, Empirical formula for dynamic biot coefficient of sandstone samples from south-west of Poland, Energies 14 (2021), https://doi.org/10.3390/en14175514.
[129] A.P.S. Selvadurai, A.P. Suvorov, The influence of the pore shape on the bulk modulus and the biot coefficient of fluid-saturated porous rocks, Sci. Rep. 10 (2020), https://doi.org/10.1038/s41598-020-75979-6.
[130] S. Yu, C.T. Oguchi, Role of pore size distribution in salt uptake, damage, and predicting salt susceptibility of eight types of Japanese building stones, Eng. Geol. 115 (2010) 226–236, https://doi.org/10.1016/j.enggeo.2009.05.007.